INTERNATIONAL JOURNAL FOR NUMERICAL AND ANALYTICAL METHODS IN GEOMECHANICS
Int. J. Numer. Anal. Meth. Geomech. 2015; **39**:2017–2036
Published online 4 May 2015 in Wiley Online Library (wileyonlinelibrary.com). DOI: 10.1002/nag.2383

Hydro-mechanical erosion models for sand production

E. Gravanis[1], E. Sarris[1,2,*,†] and P. Papanastasiou[1,2]

[1]*International Water Research Center (IWRC) NIREAS, University of Cyprus, 1678 Nicosia, Cyprus*
[2]*Department of Civil and Environmental Engineering, University of Cyprus, 1678 Nicosia, Cyprus*

SUMMARY

Sand production is a complex physical process that depends on the external stress and flow rate conditions as well as on the state of the material. Models developed for the prediction of sand production are usually solved numerically because of the complexity of the governing equations. Testing of new sand production models can very well be performed through calibration with laboratory experiments, which by construction possess geometric symmetry facilitating explicit mathematical analysis. We introduce an erosion model that is built upon the physics (poro-mechanical coupling of the fluid-solid system) usually incorporated in erosion models for the prediction of sand production. Around this model, we set up a mathematical framework in which sand production models because of erosion can be tested and calibrated without having to resort to complex numerical work or specialised software. The model is validated by data of volumetric sand production from a hollow cylinder test on synthetic sandstone. Generalisations of the model, which are naturally incorporated in the same framework and have useful phenomenological features, are discussed. Copyright © 2015 John Wiley & Sons, Ltd.

Received 18 August 2014; Revised 20 February 2015; Accepted 9 March 2015

KEY WORDS: sand production; volumetric sand prediction; erosion hydromechanics; hollow cylinder; poro-plasticity

1. INTRODUCTION

Sand erosion, in the sense that interests us in this work, is the phenomenon where a fluid saturated rock loses its mechanical integrity because of the applied stress field and is transported away in the presence of pore pressure gradients. The unintended by-product of solid particles of oil and gas production is generally referred to as sand production. In practice, the aggressive pumping of oil from the well causes grain dislocation from the solid matrix of the rock, thereby leading to mechanical problems such as accumulation of sand in the wellbore and the creation of unstable cavities in the geological formation. Particle influx into the wellbore may lead to various problems such as erosion of valves and pipelines, plugging of production liners and sand deposits in the separators. Additionally, during production, sudden erosion in high-pressure gas wells represents a major safety risk [1, 2]. The design issue that arises from this problem, and it is of considerable interest to the oil and gas operating companies, is the prediction or control of these particles.

In the view of modelling, the different processes that are involved in the sand production problem are associated with (1) fluid and solids transport; (2) fluid/rock interaction; and (3) rock deformation. Modelling of the sand production physical problem is not a trivial process as it involves the following coupled mechanisms: (a) the mechanical instabilities and localised compressional or tensile failure (damage) of the rock in the vicinity of the wellbore because of stress concentration

*Correspondence to: E. Sarris, Department of Civil and Environmental Engineering, University of Cyprus, 75 Kallipoleos street, P.O.Box 20537, 1678 Nicosia, Cyprus.
†E-mail: esarris@ucy.ac.cy

and (b) the hydro-mechanical instabilities caused from internal and surface erosion, which manifest themselves in releasing and transferring the particles caused by the action of seepage forces. These two mechanisms are coupled because the stress concentration will lead to loss of cohesion of the material causing localised damage, which in turn will increase the amount of loose solids that can leave the rock formation. This solid wash-out will bring an increase at the porosity of the intact rock as a direct effect of the localised damage and eventually will cause the inter-granular forces to re-adjust to the new configuration of the rock formation, thus leading to further damage of the rock [3].

In reality, erosion is influenced by various mechanisms. These include combinations of drawdown, drawdown rate (ramp-up strategy), depletion, flow rate, water-cut, completion strategy (size, phasing and orientation of perforations) and frequency of shut-downs and start-ups. It is evident that modelling the contribution from all these mechanisms in a single erosion model is highly complex [4–6].

It has been suggested that some limited amount of sand production can eventually lead to an increase in oil and gas production [7]. This suggestion dictates the necessity to determine the amount of sand produced after the first occurrence. This has motivated many researchers to focus on the sand prediction via numerical, analytical and experimental investigations. The availability of models to predict the onset and quantity of sand produced is very crucial. There is a vast literature in the modelling of erosion phenomena attempting to capture the failure and onset of sanding [8–19]. Sanding criteria that are routinely used in the models for predictions are usually based on shear, tensile failure [9, 10] critical pressure gradient [11], critical plastic deformation [12, 13] and erosion based criteria [14–16]. Among those contributions, the authors of Papanastasiou and Vardoulakis [20] used bifurcation theory to simulate the localised mechanical response of the reservoir rock with evolving pressure and effective stresses during the life span of the wellbore into the post bifurcation regime. They showed that the tendency for compressive or tensile failure around a cavity depends on the cavity size. Large cavities (e.g., wellbores) fail under compression at low stress level, whereas small cavities (e.g., perforations) fail under both, extension or compression at higher stress and strain level depending on the material properties.

The seminal work of Vardoulakis *et al.* [3] proposed the basic theory for hydrodynamic erosion to deal with the instabilities caused from internal and surface seepage forces on sandstone, which is based on filtration theory without solving the stress equilibrium equation. In their work, stresses and rock deformation were suppressed with emphasis put on mass transport. As an extension to that work, the authors of Papamichos and Stavropoulou [12] combined the evolution of localised deformation with hydrodynamic erosion calibrated with laboratory experiments to predict the onset and amount of solids produced as well as the production rate. Furthermore, the authors of Stavropoulou *et al.* [21] extended the approach by solving the momentum and continuity equations for fluid flow, solids and fluidised solids coupled with an elastic perfect plastic Mohr–Coulomb yield criterion to perform wellbore stability analysis after erosion. The parameters of cohesion, Young modulus, permeability and sand production coefficient were linked with the porosity through a set of calibration parameters. That was the motivation for many researchers to adopt the full strength behaviour of the material in their models [13, 22–24].

In general, standard analytical models [17, 25] provide formulations for the fluid flow rate that is required to cause compressive or tensile failure triggering the onset of sand production. The critical fluid flow rate, that onsets the phenomenon, is a function of (a) the viscosity of the permeating fluid, (b) the permeability of the rock formation and (c) the formation strength properties. Most numerical models [5, 26] deal with the coupling of the physical processes by attempting to link failure to plastic yielding through the assumption that the post peak strength is an appropriate condition for sand production and tie solids production to a mobilised critical strain level, which is determined by laboratory or field data [27, 28]. The use of this criterion requires a calibration study of every specific field or laboratory case. However, this criterion based on failed material makes progression of failure possible and release more material for production. A detailed general literature survey on sand prediction models can be found in Rahmati *et al.* [29].

This paper presents the development of a mathematical framework, in which hydro-mechanical models used for predicting sand production in weak rocks (e.g. sandstone) can be tested and calibrated. Simultaneously, a simple erosion model is introduced to operate in this framework. The model is a transcription of the model given by Papamichos *et al.* [13]. The hydro-mechanical models around our mathematics are constructed along the following line of thought.

DOI: 10.1002/nag

One starts with a basic phenomenological relation, which states that the rate of change of porosity throughout the material depends on the porosity itself and the Darcy flux of the permeating fluid [3]. This relation contains a phenomenological coefficient, which we shall call as the erosion strength coefficient λ. When λ is a constant, the basic erosion model equation and the associated models are completely hydrodynamic in nature [3, 21]. It turns out that these models cannot localise the effects of erosion near the exit surface of the flow in contrast with intuition and observations. A remedy to this problem was first suggested in Papamichos and Stavropoulou and Papamichos *et al.* [12, 13]. It is a priori expected that erosion will be stronger in high stress concentration regions. More concretely, one may conveniently associate erosion with plasticity. Adopting a certain failure criterion for the material under consideration, erosion is restricted in the region where this criterion is satisfied; that is, the erosion region is associated with the plastic region [12, 13]. This is performed by assuming that the erosion strength depends on the equivalent plastic strain in a prescribed manner. The idea is that erosive failure rests on plastic failure. Under plasticity, the material is damaged and decohesioned so that is can be eroded away under the weak hydrodynamic forces. The procedure of Papamichos and Stavropoulou and Papamichos *et al.* [12, 13] does indeed lead to a working method and reasonable localisation of the erosion effects near the exit surface.

The same physical ideas can be implemented in a mathematical description of the problem in a variety of ways. In this work, the localisation effect is introduced directly in physical space by introducing in the model equation a profile factor (a smoothed step function), which depends on the size of the plastic region. In other words, the original erosion strength λ of Vardoulakis *et al.* [3] acquires explicit space dependence so that this parameter 'knows' where the plastic region is. This is a very convenient simplification of the localisation method proposed in Papamichos and Stavropoulou and Papamichos *et al.* [12, 13], and at least equally as effective. Also, this is how the mechanics of the material is introduced in the present erosion model. Degradation of the material, which is also present in the previous versions of the erosion model, is formulated suitably to complete the coupling of the hydrodynamics with the mechanics of the material. As porosity increases in the plastic/erosion region, the material softens (degradation) and the plastic/erosion region progressively evolves deeper. The system evolves in a quasi-steady state. The material evolves through a succession of states where the equilibrium equations are applied at each step, which allows erosion poro-elastoplastic solutions for the stress field to be derived under the assumed (cylindrical) symmetry. Thus, a mathematical framework may indeed be set up, in which one can test and calibrate various erosion models without having to resort to far more complex numerical work (e.g. finite elements) and the use of specialised software.

The problem is formulated based on the hollow cylinder test geometry. The formulation of the differential equations of the erosion kinematics, fluid flow and stress equilibrium is presented in Section 2. Comparison of the model predictions with the experimental results of Papamichos *et al.* [13] is presented and discussed in Section 3. The influence of the model parameters on the erosion process are discussed in Section 4. In Section 5, the erosion strength λ is deduced from the experimental data by means of back analysis, and the findings are discussed and evaluated. In section 6, we comment on certain deficiencies of the basic erosion model and the need for a specific type of modifications required. We then introduce suitable generalised models showing that they can be naturally included in the set-up mathematical framework. A discussion on the general conclusions drawn from this work is given in Section 7.

2. COUPLED STRESS–FLUID FLOW EROSION MODEL

The coupled stress–fluid flow erosion model is developed in order to analyse the hollow cylinder test, as mentioned earlier. Figure 1 shows the 2D representation of the model. The model is cylindrically shaped with a coaxial cylindrical cavity. The fluid flows radially from the outer surface towards to hole.

Under such conditions, any deformation of the rock will take place in a plane normal to the cylinder axis. The model is loaded isotropically at the outer and inner boundaries at r_{in} and r_{out} with σ_{in} and σ_{out} respectively.

DOI: 10.1002/nag

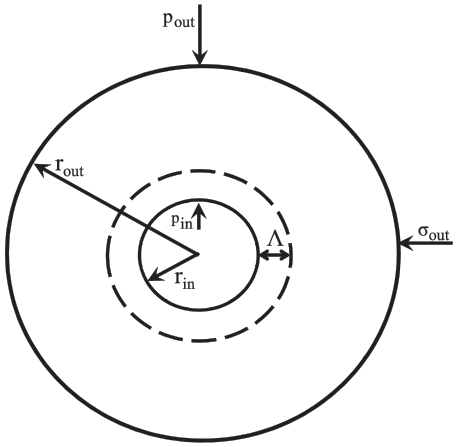

Figure 1. Schematic of the hollow cylinder problem to simulate the erosion process under radial flow.

2.1. Darcy's law and fluid mass conservation

Consider radial flow between two fixed radii, $r_{\text{in}} \leq r \leq r_{\text{out}}$, in a porous material of thickness H. Fluid mass conservation is expressed by the continuity equation:

$$\frac{\partial q_i}{\partial x_i} = 0 \tag{1}$$

Darcy's law for the flow in the porous medium reads

$$\frac{\partial p}{\partial x_i} = \frac{\mu}{k(\phi)} q_i \tag{2}$$

where q_i is defined as minus the Darcy's velocity for convenience; μ is the dynamic viscosity of the fluid and k is the intrinsic permeability of the rock, which is a function of porosity ϕ according to the Kozeny–Carman equation:

$$k = k_o \frac{\phi^3}{(1-\phi)^2} \tag{3}$$

k_o is the Kozeny–Carman permeability parameter, which is constant for a given rock. Because of the radial symmetry, the mass conservation (Eqn (1)) becomes

$$\frac{1}{r}\frac{\partial}{\partial r}(rq) = 0 \tag{4}$$

where q is radial fluid flux, with the solution

$$q = \frac{A(t)}{r} \tag{5}$$

for some function $A(t)$. The function $A(t)$ is related to the flow rate $Q(t)$ by the relation $Q(t) = 2\pi HA(t)$. The relation of $A(t)$ with the pressure drop $\Delta p = p_{\text{out}} - p_{\text{in}}$ is determined by substituting Eqn (5) in the Darcy's law and integrating between the inner and outer radii:

DOI: 10.1002/nag

$$A(t) = \frac{\Delta p}{\mu \int_{r_{\text{in}}}^{r_{\text{out}}} \frac{dr}{k(\phi)\, r}} \tag{6}$$

2.2. The erosion model

In a hydro-mechanical context, the rate of erosion is expected to depend on the porosity ϕ of the rock, the concentration of the fluidised particles and the Darcy flux q of the fluid flow, or equivalently through the Darcy law, the pressure gradient. This dependence can be set in a variety of ways. In the original reference [3], the eroded mass rate law is assumed to be proportional to the solid mass proportion $1-\phi$, the fluidised particles concentration and the Darcy flux; the proportionality constant has dimensions of inverse length. The fluidised particles concentration is a dynamical variable in Vardoulakis *et al.* [3]. In subsequent works [12, 13, 21], the analysis is simplified treating this quantity as a constant, which is absorbed in the proportionality constant of the law and eliminated from the formulas. More recent works modify this law [30–33] setting the erosion rate proportional to the pressure gradient minus a cut-off value, in order to incorporate the phenomenology of the onset of sand production more directly into the modelling. In this work, the choice of the erosion model serves mostly illustration purposes. As discussed in the introduction, we shall follow Papamichos *et al.* [13] fairly closely, adopting the basic hydro-mechanical characteristics of the erosion model used there.

The *erosion model equation* we shall use reads

$$\frac{\dot{m}}{\rho_{\text{solid}}} = \lambda \lambda_p(r,t)\,(1-\phi)^{\beta} q \tag{7}$$

where $\dot{m}$ is the rate of eroded mass production per unit volume, ρ_{solid} is the mass density of the solid matrix of the porous material and λ is a quantity with dimensions of inverse length and represents the strength of the erosive processes that lead to sand production. Parameter λ is usually called sand production coefficient, but we shall prefer the name erosion strength coefficient, or merely erosion strength. Parameter β is an exponent-parameter of the model. Parameter $\lambda_p(r,t)$ is the erosion profile function defined as follows.

The material is also subjected to fixed radial symmetric stress conditions at its inner and outer radius. Because of the imposed stress, plastic deformations are created around the hole. Let Λ be the depth of the plastic region. The $\lambda_p(r,t)$ can be any smoothed step function such that equal to 1 (unity) within the plastic zone and 0 (zero) outside. Explicitly, we require

$$\int_{r_{\text{in}}}^{r_{\text{out}}} \lambda_p(r,t)\, dr = \Lambda(t) \tag{8}$$

We choose an exponential function with these properties

$$\lambda_p(r,t) = \exp\left[-\Lambda(t)^{-a}\,[\Gamma(1+1/a)]^{a} \times (r-r_{\text{in}})^{a}\right] \tag{9}$$

($\Gamma(x)$ is the usual Euler gamma function.) The profile function $\lambda_p(r,t)$ approaches a step function as a increases. The exponent a is fixed at the beginning of the analysis, and it is not tuned further as part of the calibration procedure. In this work, we shall use $a=2$ throughout. The shape of the profile function for various values of a is shown in Figure 2.

The solid material mass conservation reads $\dot{m} = \rho_{\text{solid}} \partial\phi/\partial t$. Therefore, Eqn (7) takes the explicit form

DOI: 10.1002/nag

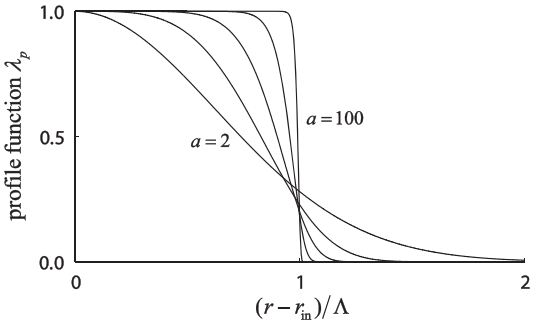

Figure 2. The erosion profile function λ_p for $a = 2$, 4, 8, 20, 100.

$$\frac{\partial \phi}{\partial t} = \lambda \lambda_p(r,t)\,(1-\phi)^{\beta} q \tag{10}$$

As implied by Eqn (8), the plastic region depth Λ changes with time as the stresses change with drawdown and depletion time. The rule under which Λ evolves will be described in the succeeding texts. The model is completed by introducing a prescribed dependence of the erosion strength λ on Λ, also given later on. One should therefore bear in mind that λ depends on time.

2.3. *Solution of the radial erosion flow*

The problem can be treated either under fixed pressure drop Δp or fixed flow rate Q. For the cases, we shall consider that the two conditions are practically equivalent. We shall work with the mathematically more interesting case of fixed pressure drop. In Section 6, we shall discuss the constant rate condition in the context of generalising the erosion model (Eqn (7)). We define the mathematical time T by

$$dT = \frac{\lambda}{\Delta r} A(t) dt \tag{11}$$

where $\Delta r = r_{out} - r_{in}$. Then the erosion model (Eqn (7)) becomes

$$\frac{\partial \phi}{\partial T} = \frac{\Delta r}{r} \lambda_p(r,T)(1-\phi)^{\beta} \tag{12}$$

Its solution reads

$$\phi(r,T) = 1 - \frac{1-\phi_0}{\left(1 + (\beta-1)(1-\phi_0)^{\beta-1} \frac{\Delta r}{r} \int_0^T \lambda_p(r,T) dT\right)^{1/(\beta-1)}} \tag{13a}$$

$$\phi(r,T) = 1 - (1-\phi_0) \exp\left[-\frac{\Delta r}{r} \int_0^T \lambda_p(r,T) dT\right] \tag{13b}$$

for $\beta \neq 1$ and $\beta = 1$ respectively. Now, everything can be calculated in terms of $\phi = \phi(r,T)$. $A(T)$ is calculated from this function by Eqn (6). The corresponding physical time is calculated by

DOI: 10.1002/nag

$$t(T) = \Delta r \int_0^T \frac{dT}{\lambda A(T)} \tag{14}$$

Then the eroded mass rate is given by

$$\dot{M} = \int \dot{m} dV = \rho_{\text{solid}} 2\pi H A(t) \lambda \int_{r_{\text{in}}}^{r_{\text{out}}} \lambda_p(r,t)(1-\phi)^\beta dr \tag{15}$$

2.4. Calculation of the plastic region depth: erosion poro-elastoplastic solutions

Once $\phi(r,T)$ is known, one may integrate Darcy's law (Eqn (2)) to obtain the evolution of the pressure profile. One finds

$$p = p_{\text{in}} + \frac{\mu}{k_o} A(T) \int_{r_{\text{in}}}^{r} \frac{(1-\phi)^2}{\phi^3} \frac{dr}{r} = p_{\text{out}} - \frac{\mu}{k_o} A(T) \int_{r}^{r_{\text{out}}} \frac{(1-\phi)^2}{\phi^3} \frac{dr}{r} \tag{16}$$

The first expression in Eqn (16), that is the one involving p_{in}, can be effectively replaced by a polynomial approximation within the erosion region; this merely requires the numerical evaluation of the integral at two or three points. Outside the erosion region, the porosity remains essentially fixed at its initial value; hence, the second expression in Eqn (16) can be evaluated explicitly. (Eqn (16) should be understood according to these simplifying observations.) Thus, all calculations involving pressure can be performed explicitly in what follows. Throughout the region $r_{\text{in}} \le r \le r_{\text{out}}$, the stress components σ_r, σ_θ satisfy the equilibrium equation:

$$\frac{d\sigma_r}{dr} + \frac{\sigma_r - \sigma_\theta}{r} = 0 \tag{17}$$

What follows should be understood in the quasi-static sense. Therefore, explicit time dependence will be left understood. The whole region is divided into a plastic region, $r_{\text{in}} \le r \le r_{\text{in}} + \Lambda$, and an elastic region, $r_{\text{in}} + \Lambda \le r \le r_{\text{out}}$ (Figure 1). In the elastic region, we have

$$\sigma_r = \alpha p + (\lambda_{\text{Lame}} + 2G)\varepsilon_r + \lambda_{\text{Lame}} \varepsilon_\theta \tag{18a}$$

$$\sigma_\theta = \alpha p + \lambda_{\text{Lame}} \varepsilon_r + (\lambda_{\text{Lame}} + 2G)\varepsilon_\theta \tag{18b}$$

where the Lame parameters are given by

$$G = \frac{E}{2(1+\nu)} \qquad \lambda_{\text{Lame}} = \frac{\nu G}{(1-2\nu)} \tag{19}$$

E is the Young modulus [MPa] and ν is the Poisson ratio [−]. The strain components (radial strain ε_r and tangential strain ε_θ) are expressed in terms of the radial displacement u by

$$\varepsilon_r = \frac{\partial u}{\partial r} \qquad \varepsilon_\theta = \frac{u}{r} \tag{20}$$

DOI: 10.1002/nag

Then, for any given pressure profile $p(r)$, the equilibrium (Eqn (17)) gives

$$u = C_1 r + \frac{C_2}{r} - \frac{\alpha}{\lambda_{\text{Lame}} + 2G}\int_{r_{\text{out}}}^{r} r' p(r') dr' \tag{21}$$

C_1 and C_2 are integration constants, which are to be determined in terms of the input data. The parameter α is the Biot coefficient, and in our explicit calculations here, we shall set $\alpha = 1$, meaning that we will neglect any compressibility effects. Employing the boundary condition $\sigma_{r\ \text{elastic}}(r_{\text{out}}) = \sigma_{\text{out}}$ eliminates the constant C_1, and one finds the expressions for the radial and tangential stresses:

$$\sigma_r = \sigma_{\text{out}} + C_2\, 2G\left[\frac{1}{r_{\text{out}}^2} - \frac{1}{r^2}\right] + \frac{\alpha 2G}{\lambda_{\text{Lame}} + 2G}\left[\frac{1}{r^2}\int_{r_{\text{out}}}^{r} r' p(r') dr'\right] \tag{22a}$$

$$\sigma_\theta = \sigma_{\text{out}} + C_2\, 2G\left[\frac{1}{r_{\text{out}}^2} + \frac{1}{r^2}\right] + \frac{\alpha 2G}{\lambda_{\text{Lame}} + 2G}\left[p(r) - \frac{1}{r^2}\int_{r_{\text{out}}}^{r} r' p(r') dr'\right] \tag{22b}$$

For the creation of the plastic region, we have considered the Mohr–Coulomb failure criterion:

$$\sigma_\theta - \alpha p = S_0 + K(\sigma_r - \alpha p) \tag{23a}$$

$$K = \tan^2\left(\frac{\pi}{4} + \frac{\Phi}{2}\right) \qquad S_0 = 2C\sqrt{K} \tag{23b}$$

where C is material cohesion [MPa], Φ is the material friction angle [^{0}] and S_0 is the uniaxial compressive strength [MPa]. Equilibrium (Eqn (17)) and the boundary condition $\sigma(r_{\text{in}}) = \sigma_{\text{in}}$ give

$$\sigma_r = \sigma_{\text{in}}\frac{r^{K-1}}{r_{\text{in}}^{K-1}} - \frac{S_0}{K-1}\left[1 - \frac{r^{K-1}}{r_{\text{in}}^{K-1}}\right] - \alpha(K-1)\left[r^{K-1}\int_{r_{\text{in}}}^{r} (r')^{-K} p(r') dr'\right] \tag{24}$$

At this stage, there are two continuity conditions and two unknowns, the integration constant C_2 and the location of the plastic zone boundary location R. The condition $\sigma_{r\text{elastic}}(R) = \sigma_{r\text{plastic}}(R)$ gives C_2 explicitly in terms of R

$$\begin{aligned} C_2\, 2G\left[\frac{1}{r_{\text{out}}^2} - \frac{1}{R^2}\right] &= \sigma_{\text{in}}\frac{R^{K-1}}{r_{\text{in}}^{K-1}} - \frac{S_0}{K-1}\left[1 - \frac{R^{K-1}}{r_{\text{in}}^{K-1}}\right] - \sigma_{\text{out}} \\ -\alpha(K-1)\left[R^{K-1}\int_{r_{\text{in}}}^{R} (r')^{-K} p(r') dr'\right] &- \frac{\alpha 2G}{\lambda_{\text{Lame}} + 2G}\left[\frac{1}{R^2}\int_{r_{\text{out}}}^{R} r' p(r') dr'\right] \end{aligned} \tag{25}$$

and

$$\sigma_{\theta\text{elastic}}(R) = \sigma_{\theta\text{plastic}}(R) \tag{26}$$

is solved numerically for R. Given the continuity of σ_r and p, the continuity of σ_θ follows from applying the Mohr–Coulomb failure criterion (Eqn (23a)) at $r = R$ also on the elastic solutions (Eqns (22a) and (22b)). Note that Eqn (26) is purely algebraic. Thus, the plastic region depth is determined, $\Lambda = R - r_{\text{in}}$.

2.5. *Degradation: Running Λ and the quasi-steady state*

The plastic region depth Λ is affected indirectly by the hydrodynamic evolution of the pressure profile, given in Eqn (16), which in turn affects the calculation of Λ, discussed in the preceding texts. This

DOI: 10.1002/nag

effect is actually small. We now come to the law under which Λ becomes dynamical in a direct manner because of the deterioration of the material caused by erosion.

By definition of the erosion profile function, we have that at any instant of time:

$$\Lambda(T)^{-1}\int_{r_{\text{in}}}^{r_{\text{out}}}\lambda_p(r,T)\,dr = 1 \tag{27}$$

which is nothing but re-writing (Eqn (8)). We use this fact to define a spatial average of the porosity:

$$\overline{\phi}(T) = \Lambda(T)^{-1}\int_{r_{\text{in}}}^{r_{\text{out}}}\lambda_p(r,T)\,\phi(r,T)dr \tag{28}$$

We introduce the running Young modulus and cohesion coefficients defined by

$$E(T) = E\frac{1-\overline{\phi}(T)}{1-\phi_0} \qquad C(T) = C\frac{1-\overline{\phi}(T)}{1-\phi_0} \tag{29}$$

expressing the degradation of the material. We assume that the friction is left unaffected by degradation. At the external confinement used in our work and Papamichos *et al.* [13], friction is possible to be mobilised and increase as a function of the plastic shear strain. However, plastic shear strains also cause deformation on the grains, causing the creation of cracks that directly reflects in a cohesion-softening behaviour. As the cementation of the natural or the synthetic sandstones gradually decreases, the cohesive strength of the material weakens. In such cases, micro-cracks develop first (which is usually the case) and it is reasonable to assume a cohesion-softening behaviour without the friction hardening. The later assumption was also considered in Stavropoulou *et al.* [21].

$\Lambda(T)$ is calculated through Eqns (16–26) using the *running* values of the material parameters. Explicitly, the system is imagined to evolve through a succession of quasi-static time-steps. In the duration of each step, the value of Λ as well as of E and C are constant and serve to determine the value of Λ associated with the next time step. Simultaneously $\phi(r,T)$ and therefore $\overline{\phi}(T)$ are calculated in each time step by Eqn (13), taking into the values of Λ of the all previous time steps, as we explain in Section 2.7. This determines also the values of E and C associated with the next time step. This rule makes the plastic region depth dynamical in a direct manner and also couples explicitly, and strongly, the hydrodynamic part of the erosion model to its material component.

One should note that the values for the Young modulus and cohesion calculated by Eqn (29) are rather nominal values through which one models the degradation of the material in order to estimate sand production. Subsequently, the derived stress and pressure fields as well as the plastic region depth are similarly approximate. These variables are rather part of an all too approximate description of erosion, starting with the model in Eqn (6) or any similar model, operating as auxiliary quantities, which provide a very rough description of the actual local physics of the erosion process.

2.6. Switching on the erosion strength λ

The erosion strength λ is the less understood part of models that involve equations similar to Eqn (7); this applies to a large proportion of the existing sand production models. (For sand production models based on different principles, more intimately related to the mechanics of the material, refer to the discussion in the review work of Rahmati *et al.* [29].) The reason why λ is poorly understood is that the associated models are primarily hydro-dynamical in nature. In fact, they are purely hydro-dynamical when λ is an absolute constant. The mechanics of the material is usually introduced by turning the erosion strength λ to a function $\lambda(\varepsilon_p)$ of the local equivalent plastic strain ε_p (e.g. refer to Rahmati *et al.* [29]). This method, introduced in Papamichos and Stavropoulou and Papamichos *et al.* [12, 13] induces association of the erosion region with the plastic region, thereby localising erosion. Simultaneously, it causes a gradual switching on of the erosion strength, modulated by the plasticity.

In the present work, localisation is effected by the profile function $\lambda_p(r,t)$, which is controlled by the depth of the plastic region. The magnitude of the erosion strength λ is still a constant. As we shall

DOI: 10.1002/nag

discuss in Section 5, λ is increasing during the initial stages of the erosion process, then reaches a stage where it can be approximated as constant, and eventually reaches a stage where it is decreasing. Therefore, the time variation of the λ must be introduced independently. Presumably, this latter stage is the most difficult to understand as it seems to be related to modes of failure of the material lying beyond the modelling of the material presented here. It is not within the scope of this work to improve the mechanics concerning the material aspect of the sand production models. Thus, and for illustration purposes only, we shall model the initial to middle stage variation of λ by introducing time dependence to λ, requiring that it depends on the running plastic region depth Λ by the following simple rule:

$$\lambda(\Lambda) = \begin{cases} \lambda_0 + (\lambda_2 - \lambda_0)\dfrac{\Lambda - \Lambda_0}{\Lambda_p - \Lambda_0}, & \Lambda \le \Lambda_p \\ \lambda_2, & \Lambda \ge \Lambda_p \end{cases} \tag{30}$$

The numbers λ_0, λ_2 and Λ_p are model parameters that must be tuned by calibration. Figure 3 shows the graphical representation of this relation.

In words, Eqn (30) expresses the following. The erosion strength starts at an initial value λ_0 and grows linearly with Λ. If Λ exceeds a (threshold) value Λ_p, then the strength λ becomes constant and equal to λ_2 (reaches a plateau). The threshold value Λ_p is quantified in terms of the initial depth Λ_0, which is calculated from the equilibrium equations using initial values of the input data (refer to also the next section). Therefore, λ is essentially a function of the ratio Λ/Λ_0.

2.7. *Solution procedure*

The formulas given in the preceding texts reduce the derivation of explicit results to the calculation of certain integrals and the solution of an algebraic equation through a series of time steps. The independent time variable is the mathematical time T. T is discretised according to a suitable time step δT; that is, we set $T = i\delta T$, where i is an integer.

At $T = 0$, the porosity field is everywhere known, $\phi = \phi_0$. Therefore, the quantity A from Eqn (6) and the pressure field from Eqn (16) are calculated easily. Then the equilibrium equations of Section 2.4 allow the determination of the initial plastic region depth $\Lambda_0 = \Lambda(T = 0)$ by solving Eqn (26).

At time $T = \delta T$, the porosity field is calculated from Eqn (13a). The formula involves the integral $\int_0^T \lambda_p(r, T)dT$, which is approximated by $\lambda_p(r,0)\ \delta T$. The profile factor $\lambda_p(r,T)$ is given by Eqn (9). The $\lambda_p(r,0)$ is then known, as $\Lambda_0 = \Lambda(T = 0)$ is known from the previous time step. The quantity A and the pressure field are calculated from Eqns (6) and (16), and the equilibrium equations provide the new value of the plastic region depth $\Lambda_1 = \Lambda(T = \delta T)$ by Eqn (26). For the latter calculation, the initial values of the Young modulus and the cohesion are used. Equations (28) and (29) allow then the calculation of the running Young modulus and cohesion, $E_1 = E(T = \delta T)$ and $C_1 = C(T = \delta T)$, to be used in the next time step along with Λ_1.

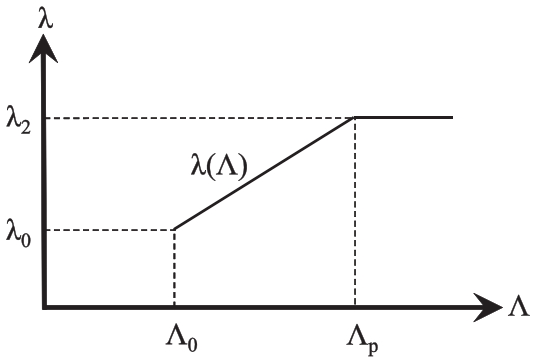

Figure 3. Graphical representation of Eqn (30).

DOI: 10.1002/nag

At the general time $T = i\delta T$, the porosity field is calculated from Eqn (13a) once the integral $\int_0^T \lambda_p(r,T)dT$ is approximated by $\{\lambda_p(r,0)+\ldots+\lambda_p(r,(i-1)\delta T)\}\delta T$. This involves the values of the depth Λ at all the previous time steps, which are known. As explained in the preceding texts, the quantity A, the pressure field and the new value of the plastic region depth $\Lambda_i = \Lambda(T = i\delta T)$ can then be calculated. By Eqns (28) and (29), the Young modulus and cohesion, $E_i = E(T = i\delta T)$ and $C_i = C(T = i\delta T)$, to be used in the next time step along with Λ_i.

Given the information collected as explained, Eqns (14) and (15) allow the translation to real time t and the calculation of sand production for all time steps. Also, the radial and tangential stresses σ_r and σ_θ can be calculated from the formulas of Section 2.4. Presumably, the discretised version of the model discussed in the preceding texts could be very well regarded as the *actual* proposed model in this work.

3. COMPARISONS BETWEEN MODEL PREDICTION AND EXPERIMENTS

In this section, we present the results from the analysis conducted for the modelling of the sand production in the hollow cylinder test problem. The rock is treated, in accordance with our formalism, as an elastic-plastic Mohr–Coulomb solid infiltrated with fluid which obeys the Darcy law.

The mechanical properties of the synthetic sandstone used in the hollow cylinder test of Papamichos *et al.* [13] were studied experimentally in Tronvoll *et al.* [2] for external stresses up to 3.5 MPa. The test presented in Papamichos *et al.* [13] involved external stresses above 7.5 MPa; for the simulations, the authors used a non-linear elastic-plastic model [30] calibrated for synthetic sandstone according to the data of Tronvoll *et al.* [2]. Here we shall use the mechanical properties of the Red Wildmoor sandstone calibrated for the Mohr–Coulomb yield criterion after the work of Sulem *et al.* [34]. Any difference between these material data and the actual data of the synthetic sandstone at the stress levels of interest will not affect qualitatively the issues of primary concern in this work; that is, whether the basic physics underlying the models in Papamichos and Stavropoulou and Papamichos *et al.* [12, 13] is maintained in the present model. Nonetheless, in Section 6, we shall return to investigate parametrically the effect of the cohesion C and friction angle Φ, which predominantly affect plasticity and therefore the sand production, through back analysis. The input and model parameters upon which the computations were performed are given in Table I.

Table I. Model properties and input data.

Variable	Value
Geometric properties	
Hollow cylinder internal radius, r_{in} [m]	0.01
Hollow cylinder external radius, r_{out} [m]	0.1
Cylinder height, H [m]	0.2
Porous rock and fluid properties	
Young modulus, E [MPa]	6750
Poisson ratio, v [−]	0.19
Cohesion, C [MPa]	3.7
Friction angle, Φ [°]	37.4
Initial porosity, ϕ_0 [−]	0.3
Initial rock permeability, k [md]	500
Solids density, ρ_{solid} [kg/m^3]	2640
Kozeny–Carman parameter, k_o [m^2]	8.956E-12
Dynamic viscosity, μ [MPa s]	5.0E-9
Model Parameters	
Erosion strength, λ [m^{-1}]	Eqn (30)
Initial erosion strength, λ_0 [m^{-1}]	0.42 λ_2
Maximum erosion strength, λ_2 [m^{-1}]	0.088
Initial plastic region depth, Λ_0 [m]	equilibrium equations
Threshold depth of the λ plateau, Λ_p [m]	1.1 Λ_0
Model exponent in Eqn (7), β [−]	1

DOI: 10.1002/nag

Based on the test conditions presented by Papamichos *et al.* [13], we have performed simulations with different external radial stresses $\sigma_{out} = 7.5$, 8, 9, 10, 11 MPa, while the radial inner stress σ_{in} was kept to zero, and to an external pressure of $p_{out} = 0.15$ MPa (with internal pore pressure p_{in} equal to zero), which corresponds to a flow rate $Q = 0.5$ l/min.

In Figure 4, the sand production curves produced by the model under the fixed pressure drop $\Delta p = 0.15$ MPa for all the different values of external radial stress are compared with the experimental data of Papamichos *et al.* [13]. All the physical parameters are taken from Papamichos *et al.* [13], while the model parameters, associated with the erosion strength λ (shown in Table I) are tuned so that to obtain a reasonable fit with the experimental data.

Most of the tuning is required in order to capture the initial stages of the process. The tuning might be slightly excessive as the data may be distorted by the gradual change of flow rate in the experiment of Papamichos *et al.* [13]. Nonetheless, we shall take the data presented in Papamichos *et al.* [13] at face value and attempt to calibrate according to them. No dependence of λ on the external stress is required: Once, the model was calibrated for a certain reference value of external stress (11 MPa), that is the predicted curve to fit reasonably well with the experimental points, thet rest of predicted curves fall in place. One should note that at 7.5 MPa, sand production declines strongly, as if there were an external stress cut off value for the initiation of sand production. One should observe this aspect of the experimental data shown in Figure 4 in conjunction with the progression of the plastic region depth Λ, as predicted by the model for the same cases, shown in Figure 5. One observes that especially at the very initial stage, the plastic region depth for the case 7.5 MPa differs by more than an order of magnitude from the depth of the next case (8 MPa), while the other four cases lie within an order of magnitude. The initial values Λ are mostly a result of the standard equilibrium equations combined with the Mohr–Coulomb criterion than of any of them are components of the model. We

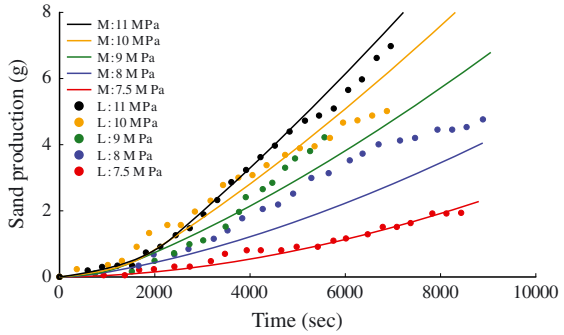

Figure 4. Comparison between the curves predicted by the model (denoted as 'M' - continuous lines) with the test data of Papamichos *et al.* [13] (denoted as 'L' – marker points) for fixed pressure drop $\Delta p = 0.15$ MPa (flow rate $Q = 0.5$ l/min).

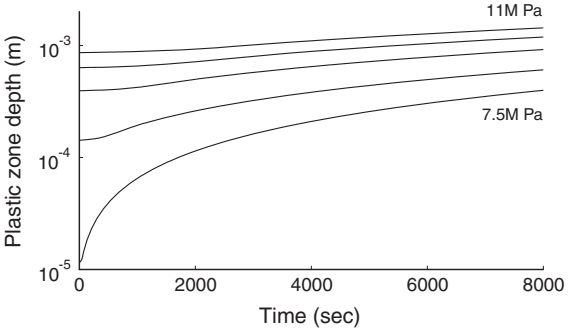

Figure 5. Progression of the plastic region depth Λ as predicted by the model for the cases of 7.5, 8, 9, 10 and 11-MPa external radial stresses.

DOI: 10.1002/nag

consider this observation as supporting the empirical basis of the localisation method of Papamichos and Stavropoulou and Papamichos *et al.* [12, 13], which we have also adopted here: Plasticity controls erosion. In regard with the late time stages of the process, one should note that the experimental curves in Figure 4 exhibit break points, that is parts of the curve where slope has decreased suddenly. This phase of the process is associated with material failure not covered by the Mohr–Coulomb criterion and therefore not described by the model.

In all, these results are in accordance with the findings of Papamichos *et al.* [13], verifying that the present model carries essentially the same physics as the one used there. The present model may have a little more freedom, as the switching on of the erosion strength λ with time, given by Eqn (30), is not modelled simultaneously with localisation, which is effected by the profile function in Eqn (7). The general statement is that hydrodynamic erosion models of the general type (Eqn (7)), which localise erosion through plasticity, perform reasonably well under different stress levels, although they are compromised because of possible additional modes of material failure during the process.

In Figure 6, we present the complete solution of the coupled hydro-mechanical erosion problem. The solution includes (a) the prediction of the cumulative sand production, the hydro-mechanical response with time of the physical fields of (b) porosity, (c) pore pressure and (d) fluid (Darcy) flux q; the mechanical response of the hollow cylinder (e) radial stress and (f) tangential stress, for the specific case of external radial stress at 11 MPa with pressure drop $\Delta p = 0.15$ MPa. The curves correspond to different stages of the erosion process differing by 1000 s. The final erosion stage is set at 9000 s.

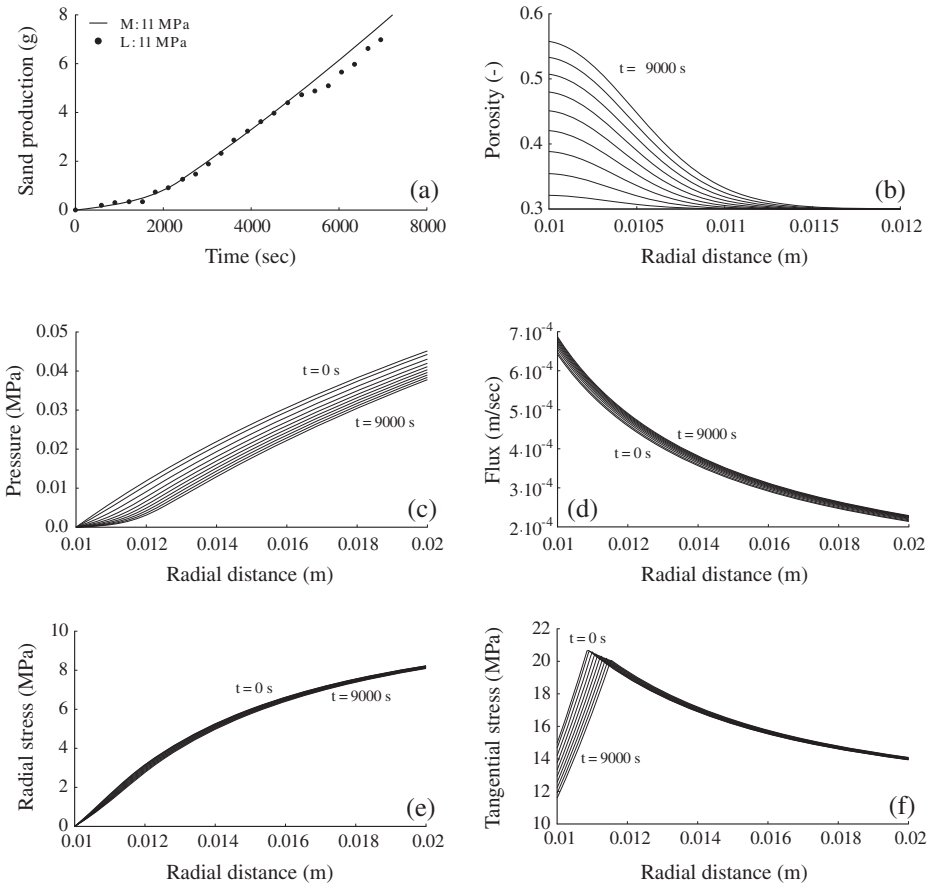

Figure 6. Sand production hydro-mechanical solution according to the proposed model for external stress level 11 MPa and pressure drop 0.15 MPa: (a) cumulative sand production, (b) porosity profiles, (c) pore pressure profiles, (d) fluid flux profiles along the hollow cylinder, (e) radial stress profiles and (f) tangential stress profiles from time 0 to 9000 s for every 1000-s interval.

DOI: 10.1002/nag

The effect of erosion is primarily encoded in the variation of the porosity field. Porosity starts from the uniform initial value 0.3 and increases near the inner hole. This causes material softening, which in turn causes the plastic region depth Λ to progress and the porosity increase advances deeper into the rock. The flattening of pressure curves observed near the hole, that is the decrease of the local pressure drop in the vicinity of the inner radius, is of course a direct effect of erosion as encoded in the porosity field (permeability increases with porosity by the Kozeny–Carman equation). Softening of the material, along with the advancement of the plastic zone, is reflected in the tangential stress solution, where stresses near the inner radius decrease significantly as a result of the coupling between hydrodynamics, plastic yielding and material degradation (softening). The effect of these three mechanisms coupled together can be described as follows. Hydrodynamics and degradation erode and soften the material, and plastic yielding provides that more material is made available for erosion and softening.

The behaviour of the erosion model (Eqn (7)) when varying the pressure drop Δp, or equivalently the flow rate Q, is summarised as follows. In Eqn (7), the local mass production is proportional to the Darcy flux. This induces a linear dependence between the total sand production and the flow rate Q. Indeed, we may introduce a time scale out of the Darcy flux (velocity) scale $(k_o/\mu)(\Delta p/\Delta r)$ and the erosion strength that has dimensions of inverse length:

$$\tau = \frac{\mu \Delta r}{\lambda k_o \Delta p} \tag{31}$$

The parameter λ in this formula may be regarded as the maximum value λ_2. Figure 7 shows the sand production curves derived by the model for different values of pressure drop, $\Delta p = 0.15, \ldots,$ 0.90 MPa with a constant external stress level of 11 MPa against the scaled time t/τ. From Figure 7, one observes that all production curves are essentially identical. The difference is mainly because of the evolving λ during the initial stage of the process. Therefore, the sand production is indeed proportional to the flow rate under the Eqn (7); that is, if we were to calibrate the model for a certain reference value of Q, then we can predict sand production for other values of the flow rate. In Papamichos *et al.* [13–28], it is argued that this proportionality is supported (very) approximately by experiment. Nonetheless, considering the data of Papamichos *et al.* [13] in scaled time t/τ suggests that this is too approximate and possibly not entirely correct, in the sense that different Q curves (for the same external stress) do not visibly collapse to each other at an acceptable level. At any rate, we shall regard the q dependence of the erosion models as an open issue. We will revisit this matter in Section 6.

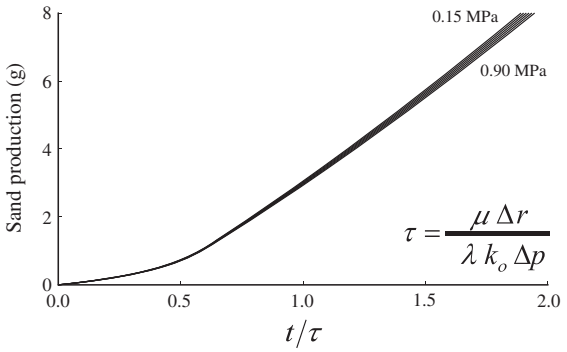

Figure 7. Predicted sand production curves for external stress 11 MPa and the different pressure drop level (different flow rate) in scaled time. The curves are practically self-similar.

DOI: 10.1002/nag

4. INFLUENCE OF MODEL PARAMETERS ON SAND PREDICTION

The model parameters are internal quantities to the model without an established physical significance. As mentioned in Section 2.6, these quantities are the initial erosion strength λ_0, the maximum erosion strength λ_2 and the threshold depth Λ_p of Eqn (30). Furthermore, it is useful to add to them the exponent β of the model (Eqn (7)) that changes the porosity of the material.

It is instructive to study the effect of these parameters on the sand production curves, that is how the shape of the curve is changed by varying the model parameters. Thus, we perturb the model parameters around the values obtained after calibrating with the case of external radial stress 11 MPa and pressure drop 0.15 MPa with the test data of Papamichos *et al.* [13]. The results from the analysis of the model parameters are shown in Figure 8. For each investigation, the model sand production curves are compared with the corresponding experimental curve.

The effect of the maximum erosion strength λ_2 (Figure 8a) and the effect of exponent β (Figure 8d) are to change the overall pace of sand production in the post-initial stage of the process, while the exponent β affects also slightly the curving. Figure 8b shows that the threshold Λ_p mostly delays the post-initial stages, and the predicted sand production curves behave in the post-initial stages as curves of smaller λ than λ_2. Finally, the initial strength λ_0, or better the fraction λ_0/λ_2, has the same effect with the threshold Λ_p parameter along with a suppression of the initial sand production.

5. EROSION STRENGTH λ FROM EXPERIMENTAL DATA

All our investigations are based on the rule governing the evolution of the erosion strength λ during the erosion process, given by Eqn (30). This is an empirical and crude way to simulate the behaviour of λ during erosion, so the model sand production curves to imitate reasonably the experimentally deduced production curves under given condition (as it is shown in Figure 4). Then, the following interesting question arises naturally. How λ need to vary over time, that is how its exact pattern looks like during the erosion process in order to produce the experimental sand production curves as model production curves?

The answer to this question can be given by means of back analysis of the experimental data. The experimental curve (i.e. the set of points) of each case studied in Section 3 may be regarded as a

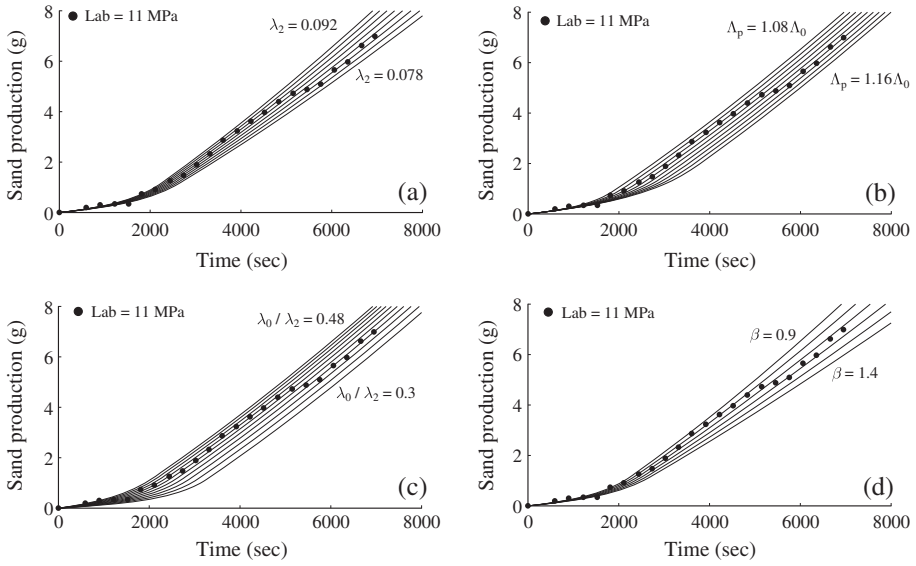

Figure 8. Influence of model parameters on the shape of the sand production curve with external stress level 11 MPa and pressure drop 0.15 MPa: (a) maximum erosion strength λ_2, (b) threshold depth Λ_p, (c) ratio of initial to maximum erosion strength λ_0/λ_2 and (d) model exponent coefficient β.

DOI: 10.1002/nag

piecewise constant sand production rate $\dot{M}$ curve, by connecting the experimental points with straight lines. Then, at each time step, λ can be deduced from Eqn (15), which is now used in the inverse way—from a known sand production curve M, we deduce λ over time. With a value of λ at hand for each time instant, one may proceed as discussed in Section 2.7.

In Figure 9, we plot the erosion strength λ and the dimensionless product $\lambda\Lambda$ (erosion strength × plastic region depth) over time, for the five cases considered in Section 3. If erosion can indeed be associated with plasticity, as it is the physical basis of erosion localisation in the type of models we use here, then $\lambda\Lambda$, which is a pure number, must necessarily be an important quantity. In the present analysis, we attempt to reveal aspects of its behaviour, in the hope that they will provide useful information for shaping an understanding of this quantity in the future. Presumably, when the exponent β of the model in Eqn (7) is set to 1, the sand production rate formula (Eqn (15)) can be written in the form

$$\dot{M} = (\lambda\Lambda)\,\rho_{\text{solid}}\,Q\left(1-\overline{\phi}\right) \tag{32}$$

using the spatial average $\overline{\phi}$ of the porosity field within the erosion region, defined in Eqn (28). Thus, the number $\lambda\Lambda$ operates as the natural erosion strength for the total sand production rate, while Eqn (7) involves the local production rate.

Inspecting the curves of the Figures 9a and 9b, one observes that both quantities, the λ and $\lambda\Lambda$ graphs exhibit an initial stage where the erosion strength increases and a final stage where the erosion strength decreases, at least as a general tendency. As mentioned in Section 2.6, the erosion strength λ is forced to partially carry the burden of the mechanics of the material. One should note that although there are strong fluctuations, the values of λ during the intermediate stage congregate somewhere below $0.1\,\text{m}^{-1}$. This is consistent with the intermediate stage value $\lambda_2 = 0.088\,\text{m}^{-1}$ (Table I), which we have used in order to obtain a reasonably good fit of the experimental curves. The $\lambda\Lambda$ curves cannot converge in the intermediate stage, because the depth Λ is different for each stress level case. Note that the excessive initial fluctuations of λ, especially for the lower values of the external stress, are explained by the small initial plastic depth Λ in those cases. Therefore, by forming the product $\lambda\Lambda$, those fluctuations are smoothed out, providing a more faithful description of the erosion strength in the initial stages than λ itself. Presumably, any model, which localises erosion through plasticity, is bound to behave in a similar way.

The previous comments are qualitative in nature. The most immediate aim of the back analysis is to reveal a general behaviour for λ, specific enough from the quantitative point of view, so that to be able to improve the postulated rule $\lambda(\Lambda)$ of Section 2.6, or simply replace it with something more appropriate. The difficulty with this idea is that fluctuations are large and the intervals of Λ for each stress level differ significantly and there is no reliable way to obtain a working approximation for the evolution of λ from these data.

On the other hand, back analysis may be used to investigate the effect of varying the input parameters on the estimation of λ when the values of these parameters are poorly known or poorly estimated. As discussed in Section 3, this is the case of the parameters we have used in this work, which describe the mechanical properties of the synthetic sandstone of the hollow cylinder test of Papamichos *et al.* [13]. Thus, we calculate the mean value of λ (over its course of evolution) for the

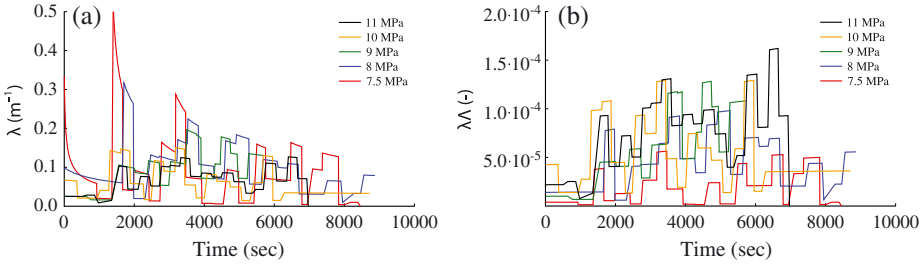

Figure 9. Behaviour of (a) erosion strength and (b) product of erosion strength with plastic zone depth with respect to time.

DOI: 10.1002/nag

cases $\sigma_{out} = 7.5$ and 11 MPa (minimum and maximum external stress) for a range of values of the cohesion C and friction angle Φ. The result is shown in Figures 10a and 10b for the minimum and maximum value of external stress respectively. We have considered values from 15 to 50° for the friction angle and values from 3 to 5 MPa for the cohesion. The curves shown in Figure 10 are labelled by cohesion values that differ by 0.2 MPa.

The larger the values of the cohesion C and the friction angle Φ are the more the material resists to plasticity. Hence, as these values increase, the plastic region depth decreases, leading to a decrease in sand production. Consulting Figure 5, we may recall that the initial value of the plastic region depth Λ_0 for the case $\sigma_{out} = 7.5$ MPa is much lower than the value of Λ_0 for the cases of $\sigma_{out} = 8$ MPa and higher (for the C and Φ values quoted in Table I). This is consistent with the findings of Papamichos *et al.* [13] that at 7.5-MPa external stress, the sand production drops significantly (as shown by the data in Figure 1). It is therefore reasonable to continue the curves in Figure 10 until the initial plastic region depth drops below a certain reference value, which is regarded as the minimum plasticity for sand production (which we set rather arbitrarily to 5×10^{-6} m, consulting again Figure 5). Based on these remarks, the first result obtained from Figure 10a is that the values of C and Φ along the notional line formed by the endpoints of the curves correspond to very small sand production. Hence, we conclude that the actual values of the cohesion and friction angle must be along, or in the vicinity of that notional line. Secondly, one observes that for the entire range of both parameters along this line, the mean value of λ lies roughly between 0.07 and 0.105 m^{-1}; that is, there is no significant deviation from the value 0.088 m^{-1} (for the maximum erosion strength λ_2) we found in the preceding texts through calibration for the C and Φ values quoted in Table I.

In Figure 10b, there is a sequence of points where the curves of same C for the two different external stress levels cross each other. At such points, the same value of mean λ is obtained for both external stress levels when calibrating with the same values of C and Φ, as we have performed previously with the values quoted in Table I. It is almost needless to say that the same, or at least, roughly the same value of mean λ should arise for different stress levels if an erosion model is to be useful at all. The mean λ values obtained this way range from 0.025 to 0.09 m^{-1}. This is a relatively large range, suggesting that one must calibrate with a different set of C and Φ values for the different external stress levels. However, by the same token, if one insists on a λ value between 0.07 and 0.105 m^{-1}, which seems to be suggested by the analysis of $\sigma_{out} = 7.5$ MPa case, there is a fairly large range of C and Φ values consistent with those values of λ in the $\sigma_{out} = 11$ MPa case. The actual values of C and Φ for the 11-MPa external stress may very well be within that range, most possibly towards the large C end.

6. GENERALISATIONS OF THE EROSION MODEL AND EXTENSION OF THE WORK

We have studied the erosion problem using the model given by Eqn (7) under fixed pore pressure difference between the inner and outer radius of the hollow cylinder test. As mentioned in Section 2.3, the problem could have been equally well solved under fixed radial flow rate Q. Adopting the

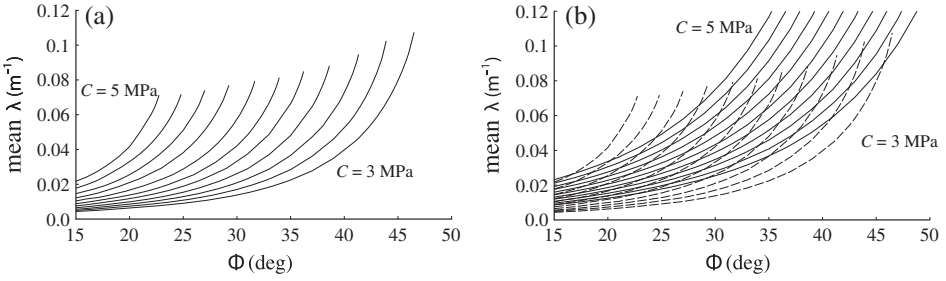

Figure 10. Mean value of erosion strength λ for the cases (a) $\sigma_{out} = 7.5$ MPa and (b) 11 MPa. The curves are labelled by the values of the cohesion C in range 3–5 MPa differing by 0.2 MPa. The curves of the case (a) are also plotted in dashed line for comparison with the case (b).

DOI: 10.1002/nag

fixed Q condition, the solution given by Eqn (13) can be written directly in the physical time t. This, in turn, allows treating more general erosion models.

Let us generalise the model (Eqn (7)) as follows:

$$\frac{\dot{m}}{\rho_{\text{solid}}} = \lambda \lambda_p(r,t)(1-\phi)^{\beta} f(q) \tag{33}$$

where $f(q)$ is a suitably chosen function of the Darcy flux q. For example, we may set $f(q) = q - q_{\text{cr}}$ for $q > q_{\text{cr}}$ otherwise 0, with q_{cr} being a cut-off for the flux densities under which erosion may occur. Clearly, q_{cr} is an additional model parameter. Models of this kind have been suggested and employed in the simulations of sand production in the recent works of Detournay *et al.*, Detournay, Papamichos, and Azadbakht *et al.* [30–33]. For constant flow rate Q, the Darcy flux (refer to Eqn (5) in Section 2.3)

$$q = \frac{Q}{2\pi H r} \tag{34}$$

is independent of time. Then the counterpart of solution (Eqn (13a)) in the present model reads

$$\phi(r,t) = 1 - \frac{1-\phi_0}{\left(1 + (\beta-1)(1-\phi_0)^{\beta-1} f\left(\frac{Q}{2\pi H r}\right) \int_0^t \lambda(\Lambda)\lambda_p(r,t)dt\right)^{1/(\beta-1)}} \tag{35}$$

The production rate formula (Eqn (15)) also becomes

$$\dot{M} = \rho_{\text{solid}} 2\pi H \lambda \int_{r_{\text{in}}}^{r_{\text{out}}} \lambda_p(r,t)(1-\phi)^{\beta} f\left(\frac{Q}{2\pi H r}\right) r dr \tag{36}$$

Only obvious modifications are required in the formalism of Section 2 in order conform to the new relations (Eqns (33–36)). The interesting attributes of the model given by Eqn (33) can be described as follows.

In Section 3, we discussed the linearity of the model given by Eqn (7) with respect to the Darcy flux q as a possibly weak characteristic of the model. Detailed work is then required to show that the generalised model (Eqn (33)), for any specific choice of function f, performs well. That is, one should examine whether the predicted sand production agrees well with the experiments for different flow rates Q, while maintaining the erosion strength λ and the additional model parameters, such as q_{cr}, independent of Q. At any rate, the novelty of the model (Eqn (33)), that is the non-trivial dependence on q, seems to be the right way to proceed. We shall defer the analysis of such models to future work.

7. SUMMARY AND COMMENTS

In the present study, we analyse the problem of sand production. We introduce an erosion model based on coupling hydrodynamic erosion with mechanical deformation of the rock under external stress. The two processes are linked by softening of the material; that is, the elastic stiffness and the cohesion of the rock are modelled to decrease with increasing porosity. In this description, sand production initiates as the material near the surface of the inner cavity fails mechanically by the applied stress field. The failed material erodes away while softening progresses deeper into the rock making more material available for erosion. The introduced hydro-mechanical erosion model while maintaining the physics usually incorporated in erosion models presents the advantage that it is more susceptible to detailed mathematical analysis. As a result, a mathematical framework is set up from which the explicit results can be deduced with relative ease, that is without the need to employ advanced numerical methods or use specialised software.

DOI: 10.1002/nag

For calibration and validation purposes, we set the theoretically derived sand production curves against experimental data. The performance of the model rests on the dependence of the erosion strength λ on the plastic zone depth Λ, discussed in Section 2.6. The dependence of λ on plasticity parameters is *not* necessary for the hydro-mechanical coupling in the present model; it only serves of additional flexibility. The function $\lambda(\Lambda)$ involves three free parameters that are to be tuned by calibration. The results show reasonable agreement between predictions and experiment. This analysis verifies the claim that the basic physical ideas usually incorporated in hydro-mechanical models have been successfully embodied in the present model.

The dependence of the erosion strength λ on plasticity parameters, in our case the plastic zone Λ, carries information about the effect of the mechanical deformations on erosion not covered by the hydro-mechanical coupling. This is why λ must be a dynamical variable and not an absolute constant. The variation of λ with time can be read off from the experimental data by back analysis. Performing this analysis, we find that λ exhibits a tendency to increases during the early stages of erosion and decrease during the late stages. Although the experimental noise is large and no definite general behaviour of λ can be deduced from the results of this analysis, the results themselves can be practically useful as tabulated information about the material under a given set of conditions.

One particular weakness about the type of the hydro-mechanical sand production models we consider here is their behaviour under different fluid flow rate conditions, that is that they behave linearly: The sand production is practically proportional to the fluid flow rate, which—in the best case—is a crude approximation of actual sand production. We suggest generalisations of the model that may have sufficient structure to deal with this difficulty and point out that these more general models can be equally well accommodated in the constructed mathematical framework. Detailed examination of their performance is left for future work.

ACKNOWLEDGEMENTS

«This work was co-funded by the European Regional Development Fund and the Republic of Cyprus through the Research Promotion Foundation (Strategic Infrastructure Project ΝΕΑΥΠΟΔΟΜΗ/ΣΤΡΑΤΗ/0308/09)».

REFERENCES

1. Tronvoll J, Fjaer E. Experimental study of sand production from perforation cavities. *International Journal of Rock Mechanics and Mining Sciences and Geomechanical Abstracts* 1994; **31**(5):393–410.
2. Tronvoll J, Skjaerstein A, Papamichos E. Sand production: mechanical failure or hydrodynamic erosion. *International Journal of Rock Mechanics and Mining Sciences* 1997; **34**(3/4): paper No. 291.
3. Vardoulakis I, Stavropoulou M, Papanastasiou P. Hydro-mechanical aspects of the sand production problem. *Transport in Porous Media* 1996; **22**:225–244.
4. Vaziri H, Xiao Y, Islam R, Nouri A. Numerical modelling of seepage induced sand production in oil and gas reservoirs. *Journal of Petroleum Science and Engineering* 2002; **36**:71–86.
5. Nouri A, Vaziri H, Kuru E, Islam R. A comparison of two sanding criteria in physical and numerical modelling of sand production. *Journal of Petroleum Science and Engineering* 2005; **50**:55–70.
6. Nouri A, Vaziri H, Belhaj H, Islam R. Sand production prediction: a new set of criteria for modelling based on large scale transient experiments and numerical investigation. *SPE Journal* 2006; **11**(2):227–237.
7. Fjaer E, Cerasi P, Papamichos E. Modelling the rate of sand production. ARMA/NARMS 2004-588. Gulf Rocks 2004, Huston, June 5-9.
8. Wang J, Wan RG. Computation of sand fluidization phenomena using stabilized finite elements. *Finite Elements in Analysis and Design* 2004; **40**:1681–1699.
9. Morita N, Whitfill DL, Massie I, Knudsen TW. Realistic sand production prediction: numerical approach. *SPE Production Engineering Journal* 1989; **16989**:15–24.
10. Morita N, Whitfill DL, Fedde OP, Lovik TH. Parametric study of sand production prediction: analytical approach. *SPE Production Engineering Journal* 1989; **16990**:25–33.
11. Bratli RK, Risnes R. Stability and failure of sand arches. *SPE Journal* 1981; **21**(2):236–248.
12. Papamichos E, Stavropoulou M. An erosion-mechanical model for sand production rate prediction. *International Journal of Rock Mechanics and Mining Sciences and Geomechanical Abstracts* 1998; **35**(4):531–532.
13. Papamichos E, Vardoulakis I, Tronvoll J, Skjaerstein A. Volumentric sand production model and experiment. *International Journal for Numerical and Analytical Methods in Geomechanics* 2001; **25**:789–808.
14. Vardoulakis I, Papamichos E. A continuum theory for erosion in granular media. *Rivista Italiana Di Geotehnica* 2003; **3**:83–90.

DOI: 10.1002/nag

15. Papamichos E, Vardoulakis I. Sand erosion with a porosity diffusion law. *Computers and Geotechnics* 2005; **32**:47–58.
16. Vardoulakis I, Papanastasiou P, Stavropoulou M. Sand erosion in axial flow conditions. *Transport in Porous Media* 2001; **45**:267–281.
17. Risnes R, Bratli RK, Harsrud P. Sand stresses around a wellbore. *SPE Journal* 1982; **22**(6):883–898.
18. Morita N, Burton RC, Davis E. Fracturing, frac packing and formation failure control: can screenless completions prevent sand production? *SPE Drilling and Completion* 1998; **13**(3):157–162.
19. Vaziri H, Wang X, Palmer I. Wellbore completion technique and geotechnical parameters influencing gas production. *Canadian Geotechnical Journal* 1997; **34**:87–101.
20. Papanastasiou P, Vardoulakis I. Numerical treatment of progressive localization in relation to borehole stability. *International Journal for Numerical and Analytical Methods in Geomechanics* 1992; **16**:389–424.
21. Stavropoulou M, Papanastasiou P, Vardoulakis I. Coupled wellbore erosion and stability analysis. *International Journal for Numerical and Analytical Methods in Geomechanics* 1998; **22**:749–769.
22. Nouri A, Vaziri H, Kuru E, Islam R. A comparison of two sanding criteria in physical and numerical modelling of sand production. *Journal of Petroleum Science and Engineering* 2006; **50**:55–70.
23. Vaziri H, Nouri A, Hovem K, Wang X. Computation of sand production in water injectors. *SPE Production and Operations* 2008; **23**(4):518–524.
24. Nouri A, Kuru E, Vaziri H. Elastoplastic modelling of sand production using fracture energy regularization method. *Journal of Canadian Petroleum Technology* 2009; **48**(4):64–71.
25. Vaziri H. Analytical and numerical procedures for analysis of flow-induced cavitation in porous media. *International Journal for Computers and Structures* 1995; **54**(2):223–238.
26. Wan RG, Wang J. Analysis of sand production in unconsolidated oil sand using a coupled erosional-stress-deformation model. *Journal of Canadian Petroleum Technology* 2002; **43**(2):47–53.
27. Fattahpour V, Moosavi M, Mehranpour M. An experimental investigation of the effect of rock strength and perforation size on sand production. *Journal of Petroleum Science and Engineering* 2012; **86-87**:172–189.
28. Papamichos E, Tronvoll J, Skjaerstein A, Unander TE. Hole stability of red Wildmoor sandstone under anisotropic stresses and sand production criterion. *Journal of Petroleum Science and Engineering* 2010; **72**:78–92.
29. Rahmati H, Jafarpour M, Azadbakht S, Nouri A, Vaziri H, Chan D, Xiao Y. Review of sand production prediction models. *Journal of Petroleum Engineering* 2013. doi:10.1155/2013/864981.
30. Detournay C, Tan C, Wu B. Modeling the mechanism and rate of sand production using FLAC, in Numerical Modeling in Geomechanics – 2006 (CD Proceedings, 4th International Symposium, Madrid, May 2006), Paper No. 08-10. R. Hart and P. Varona, Eds. Minneapolis, Minnesota: Itasca Consulting Group, Inc., 2006.
31. Detournay C. Numerical modeling of the slit mode of cavity evolution associated with sand production. CD Proceedings, SPE Annual Technical Conference & Exhibition (Denver, September 2008), Paper No. SPE 116168. Houston: SPE, 2008.
32. Papamichos E. Erosion and multiphase flow in porous media: application to sand production, 21th Alert Graduate School, October 2010. *Mathematical modelling in geomechanics (European Journal of Environmental and Civil Engineering)* 2010; **14**:1129–1154.
33. Azadbakht S, Jafarpour M, Rahmati H, Nouri A, Vaziri H, Chan D. A numerical model for predicting the rate of sand production in injector wells. Proceedings of the SPE Deep Water and Completions Conference and Exhibition, pp. 20–21, Galveston, Texas, USA, June 2012.
34. Sulem J, Vardoulakis I, Papamichos E, Oulahna A, Tronvoll J. Elasto-plastic modelling of Red Wildmoor sandstone. *Mechanics of Cohesive-Frictional Materials* 1999; **4**:215–245.

DOI: 10.1002/nag